

## Article

# Influence of Radioactive Sludge Content on Vitrification of High-Level Liquid Waste

Shengheng Tan <sup>1,\*</sup>, Jiong Chang <sup>1</sup>, Xiao Liu <sup>1</sup>, Shikuan Sun <sup>2</sup>, Liang Xian <sup>1</sup> and Shengdong Zhang <sup>1,\*</sup><sup>1</sup> Department of Radiochemistry, China Institute of Atomic Energy, Beijing 102413, China<sup>2</sup> School of Materials Science and Energy Engineering, Foshan University, Foshan 528000, China

\* Correspondence: tanshengheng@ciae.ac.cn (S.T.); zhangsd@ciae.ac.cn (S.Z.)

**Abstract:** The radioactive sludges formed at the bottom of high-level liquid waste (HLW) storage tanks pose challenges when the HLWs are vitrified. This study aims to determine the influence of the sludge content (enriched in Na<sub>2</sub>O, Al<sub>2</sub>O<sub>3</sub>, NiO, Fe<sub>2</sub>O<sub>3</sub>, and BaSO<sub>4</sub>) on the structure and properties of waste glasses in order to find the optimal ratio of sludges to HLW during vitrification. In the experiments, the simulated sludge and simulated HLW were mixed at different ratios from 0:8 to 4:4, with an overall waste content of 16 wt %, in a borosilicate glass wasteform. It is found that the glass density, molar volume, sulfur retention, and glass transition temperature changed little when increasing the sludge content of the glasses, while the viscosity, chemical durability, and crystallization features of the glasses varied notably. The crystals formed in the glasses during the thermal treatment were exclusively Fe-substituted diopside (Ca, Mg, Fe)<sub>2</sub>Si<sub>2</sub>O<sub>6</sub>. An increase in the Al<sub>2</sub>O<sub>3</sub> and NiO content of the glasses may have been responsible for the increased crystallinity at high temperatures. The leaching rate of Si, B, Na, and Cs from the glasses declined with the increasing addition of sludge to the glasses. Although all the glasses fulfilled the requirements for vitrification processing and glass-product performance, it is recommended that the sludge content of the whole waste should not exceed 25 wt %. This study guides further research on the immobilization of high-level sludges.

**Keywords:** high-level liquid waste; radioactive sludge; vitrification; glass crystallization



**Citation:** Tan, S.; Chang, J.; Liu, X.; Sun, S.; Xian, L.; Zhang, S. Influence of Radioactive Sludge Content on Vitrification of High-Level Liquid Waste. *Sustainability* **2023**, *15*, 4937. <https://doi.org/10.3390/su15064937>

Academic Editors: Michael I. Ojovan, Vladislav A. Petrov and Sergey V. Yudin

Received: 30 January 2023

Revised: 7 March 2023

Accepted: 8 March 2023

Published: 10 March 2023



**Copyright:** © 2023 by the authors. Licensee MDPI, Basel, Switzerland. This article is an open access article distributed under the terms and conditions of the Creative Commons Attribution (CC BY) license (<https://creativecommons.org/licenses/by/4.0/>).

## 1. Introduction

High-level liquid waste (HLW) from the reprocessing of spent nuclear fuels is highly radioactive, toxic, and mobile; thus, it is extremely detrimental to human beings and the environment. Therefore, to achieve the sustainable development of nuclear energy, HLWs must be appropriately immobilized into reliable hosts before geological disposal. Vitrification is recognized worldwide as the primary choice for immobilizing high-level nuclear waste [1]. Among the vitrification technologies developed so far, Joule-heated ceramic melter (JHCM) technology is the most widely applied and borosilicate glasses are the most commonly used immobilization hosts [2,3]. China operated a vitrification plant, i.e., the Vitrification Plant of China (VPC), since 2021 to produce borosilicate nuclear-waste glasses based on JHCM technology for the immobilization of legacy HLWs generated at early ages.

These legacy HLWs are usually rich in Na, Fe, Al, and S, with some traces of Ln and U [4,5]. During their long-term storage in tanks, various insoluble substances can form due to hydrolysis and salt precipitation, and the precipitates gradually sink into the bottom to form sludge layers [6]. Because the sludges are categorized as high-level nuclear waste due to their significant content of radioactive cesium and actinides, they must be immobilized into reliable matrices for deep geological disposal. Ideally, these sludges should be vitrified with the liquid HLW during the operation; however, because of the significant differences between the compositions of sludges and liquid HLWs, blending them may have significant effects on the vitrification process and the properties of borosilicate waste glasses. Furthermore, vitrifying radioactive sludges alone is also considered a possible method for

the treatment of these sludges; however, the waste loading is limited by the formation of sulfates and spinels in glass melts, according to our preliminary results. Similar sludges are also abundant at the Hanford sites in the USA, and both glass and ceramic waste forms have been developed to immobilize sludges alone [7–9]. In addition, many studies have focused on the thermal treatment of other types of radioactive sludge, such as Magnox sludge [10,11] and Fukushima sludge [12], to form glass or ceramic wasteforms.

Unlike HLWs, sludges are prone enrichment in some specific elements. In this study, the targeted sludge was composed of  $\text{Na}_2\text{O}$ ,  $\text{Al}_2\text{O}_3$ ,  $\text{Fe}_2\text{O}_3$ ,  $\text{NiO}$ ,  $\text{La}_2\text{O}_3$ ,  $\text{BaO}$ , and  $\text{SO}_3$ , with  $\text{Al}_2\text{O}_3$ ,  $\text{NiO}$ , and  $\text{BaO}$  contents much higher than those of legacy HLWs. Furthermore,  $\text{Al}_2\text{O}_3$  is a common component in nuclear waste glasses. Functioning as a network former at low contents, it usually gives rise to enhanced glass-network connectivity and chemical durability, but with an increased crystallization tendency and viscosity [13–16]. Nickel(II) oxide is not commonly found in borosilicate glasses; it is reported to be present as nanoparticles within glass matrices, and the doping of  $\text{NiO}$  could lead to increased glass crystallization [17,18]. Furthermore,  $\text{BaO}$  has been introduced to nuclear-waste glass to improve sulfate solubility, although it may result in deteriorated glass-chemical durability [5,19]. When these differences are combined, the influences might be complex and should be further investigated.

This study is part of a research project whose aim is to develop glass formulations for the vitrification of radioactive HLW sludges. The study investigates the influence of sludge contents on the structure and properties of borosilicate-nuclear-waste glasses by mixing simulated sludges with HLW simulants at different ratios to produce a series of glasses containing varying sludge contents. It then investigates the changes in the glass properties using these variations.

## 2. Materials and Methods

### 2.1. Raw Materials

#### 2.1.1. Simulated HLW and Sludge

This study used inactive waste simulants instead of natural waste. The chemical compositions of the HLW simulants in Table 1 originated from our previous paper [20], representing a natural HLW stream to be vitrified in China. During this study, a few minor components were omitted to simplify the experiments. The compositions of the simplified sludge simulants are also listed in Table 1. In order to evaluate the influence of sludge additions to HLW, the sludge simulant was mixed with HLW simulant at a ratio of 0:8, 1:7, 2:6, 3:5, and 4:4 (on an oxide basis), with the overall waste loaded constantly at 16.0 wt % in the glass.

**Table 1.** The chemical composition of the simulated HLW and sludge.

Simulated HLW		Simulated Sludge	
Oxide	Content (wt %)	Oxide	Content (wt %)
$\text{CeO}_2$	0.35		
$\text{Cr}_2\text{O}_3$	2.02		
$\text{Cs}_2\text{O}$	0.09		
$\text{K}_2\text{O}$	0.61		
$\text{La}_2\text{O}_3$	11.63	$\text{La}_2\text{O}_3$	5.0
$\text{Fe}_2\text{O}_3$	21.46	$\text{Fe}_2\text{O}_3$	20.0
$\text{Al}_2\text{O}_3$	8.77	$\text{Al}_2\text{O}_3$	25.0
$\text{BaO}$	0.13	$\text{BaO}$	5.0
$\text{Na}_2\text{O}$	45.41	$\text{Na}_2\text{O}$	20.0
$\text{MoO}_3$	0.78		
$\text{Nd}_2\text{O}_3$	0.69		
$\text{NiO}$	2.56	$\text{NiO}$	20.0
$\text{P}_2\text{O}_5$	0.44		
$\text{SO}_3$	4.62	$\text{SO}_3$	5.0
$\text{SrO}$	0.05		
$\text{TiO}_2$	0.32		
$\text{Y}_2\text{O}_3$	0.09		
Total	100.00	Total	100.00

### 2.1.2. Basic Glass

The basic glass was composed of 53.44 wt % SiO<sub>2</sub>, 14.60 wt % B<sub>2</sub>O<sub>3</sub>, 4.40 wt % Al<sub>2</sub>O<sub>3</sub>, 2.60 wt % Li<sub>2</sub>O, 5.21 wt % Na<sub>2</sub>O, 5.20 wt % MgO, 8.00 wt % CaO, 4.16 wt % BaO, 1.79 wt % V<sub>2</sub>O<sub>5</sub>, and 0.60 wt % Sb<sub>2</sub>O<sub>3</sub>, which was identical to the proportion currently used in the VPC project [20]. The basic glass contributed to 84.0 wt % of the final glass composition.

### 2.2. Glass Preparation

The glasses were labeled NJ $n$ , namely NJ0, NJ1, NJ2, NJ3, and NJ4, where  $n$  denotes the ratio of the sludge to the sum of the sludge and HLW. All the HLW simulants, sludge simulants, and primary glasses were made from the corresponding oxides, carbonates, and sulfates of analytic-grade purity purchased from Beijing Sinopharm Co. Ltd., Beijing, China.

Appropriate amounts of chemicals were weighed to make 300 g glass products, which were then mixed and mechanically homogenized for 20 min. The batches were placed in corundum crucibles and heated in an electric furnace subjected to the following heating profile: 1 h from room temperature to 200 °C, 4 h from 200 to 1150 °C, and 3 h retention at 1150 °C. Subsequently, the glass melts were poured into a preheated graphite mold and annealed in an annealing furnace at 500 °C for 1 h before the furnace was turned off.

### 2.3. Sample Characterization

Part of the as-cast glasses was crushed into pieces for glass-viscosity measurement, which was carried out with a Brookfield DV2T Viscometer equipped with an electric furnace for heating. The measurement started at 1150 °C and ended at 950 °C, with an interval of 50 °C and a period of about 10 min for temperature stability. The rotor speed was adjusted to keep the torque range constant at 40–50%. The viscometer was calibrated with a borosilicate-glass standard prior to use.

Part of the as-cast glasses was crushed and ground into fine powders ( $\leq 75 \mu\text{m}$ ) for X-ray diffraction (XRD), X-ray fluorescence (XRF), and differential scanning calorimetry (DSC) analyses. The XRD analysis was performed on a Bruker D8 Advance X-ray diffractometer operating at 40 kV and 40 mA (CuK $\alpha$ ), with a  $2\theta$  angle of 10°–70°, a step size of 0.02°, and a dwell time of 0.4 s. The XRF was employed to analyze glass compositions with an ARL Advant XP+ X-ray fluorescence spectrometer (Thermo Scientific, Waltham, MA, USA). The DSC curves were recorded with a Netzsch STA 449 F3 Thermal Analyzer, from room temperature to 1000 °C, at a heating rate of 10 °C·min<sup>-1</sup>, under a nitrogen flow. Glass powders between 75 and 150  $\mu\text{m}$  were collected for chemical-durability analysis (the performance-consistency test, PCT-B). The experiments followed the procedures described in ASTM 1285-14: the glass powders were immersed in deionized water in poly(tetrafluoroethylene) (PTFE) vessels for 7 days at 90 °C with a ratio of the surface area to the leachant volume of  $1200 \pm 50 \text{ m}^{-1}$ . The concentrations of Si, B, Na, Cs, and other elements in the leachant after leaching were measured using inductively coupled plasma–atomic emission spectroscopy (ICP–AES) or inductively coupled plasma–mass spectrometry (ICP–MS).

The crystallization behaviors and the liquidus temperatures of the glasses were analyzed by the isothermal-heat-treatment method following ASTM C1720-17. Fine glass powders (~5 g) were placed in a Pt95-Rh5 disk, covered by a Pt95-Rh5 cap, and heated in an annealing furnace for 24 h in a temperature range of 850–1025 °C using intervals of 25 °C. The heating period of 24 h was selected to allow sufficient time for crystal growth within glasses. However, it should be noted that the crystallization process did not necessarily reach equilibrium during this period. After the heat treatment, the samples were taken out of the furnace and cooled to room temperature in the air. The samples were cut diagonally into two halves, one for the XRD analysis and the other for the scanning-electron microscopy (SEM) observation. The XRD analysis was identical to that mentioned above; the fraction of the crystals in the glass was calculated based on the Rietveld refinement method using CaF<sub>2</sub> as the internal standard and the GSAS EXPGUI interface. The SEM observations were performed on polished glass pieces mounted into epoxy resin and polished with 1  $\mu\text{m}$  of diamond suspension using an FEI Inspect Quanta650 scanning-electron microscope equipped with an energy-dispersive X-ray

spectrometer (EDXS, Oxford Instruments, Abingdon, UK). The polished samples were coated with gold prior to analysis to allow electric conductivity.

### 3. Results

#### 3.1. Appearance and Homogeneity

The prepared glasses (NJ0–NJ4) were visibly homogeneous. While the bulk of all the glasses appeared dark green, the color of the powdered-glass samples gradually changed from light yellow to yellow-brownish with the addition of the sludge content. The color changes in the glass products are attributable to the high content of transition metals, such as Fe ( $\text{Fe}_2\text{O}_3$ ) and Ni ( $\text{NiO}$ ), in the sludge. Meanwhile, according to Figure 1, all the glasses were X-ray-amorphous, and the various samples differed negligibly.

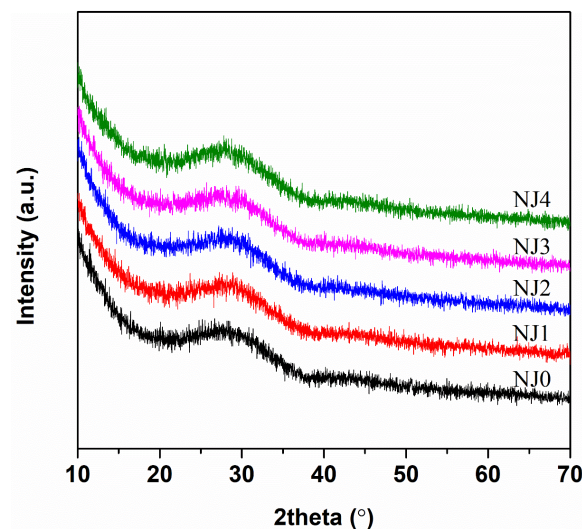


Figure 1. The XRD patterns of prepared glasses NJ0–NJ4.

#### 3.2. Glass Composition and Density

The prepared glasses were compositionally close to the nominal values, as listed in Table 2. The higher-than-expected  $\text{Al}_2\text{O}_3$  content ( $\sim 1$  wt %) is likely to have arisen through the corrosion of corundum crucibles during the glass melting, while the lower-than-expected  $\text{Na}_2\text{O}$  content might have been due to the evaporation of the glass batches and glass melts at high temperatures. Furthermore, the gaps between the nominal and measured  $\text{Al}_2\text{O}_3$  contents were similar among all the glasses, suggesting that the corrosivity of glass melts is not affected by the addition of sludge content.

Table 2. The nominal and XRF-measured normalized glass compositions (wt %).

Oxide	NJ0		NJ1		NJ2		NJ3		NJ4	
	Nominal	Measured								
$\text{SiO}_2$	44.89	45.20	44.89	44.70	44.89	45.25	44.89	44.76	44.89	44.60
$\text{B}_2\text{O}_3$ *	12.26	12.26	12.26	12.26	12.26	12.26	12.26	12.26	12.26	12.26
$\text{Al}_2\text{O}_3$	5.10	6.15	5.43	6.44	5.75	6.74	6.08	6.99	6.40	7.23
$\text{Li}_2\text{O}$ *	2.18	2.18	2.18	2.18	2.18	2.18	2.18	2.18	2.18	2.18
$\text{Na}_2\text{O}$	11.65	11.10	11.14	10.67	10.63	10.11	10.12	9.78	9.61	9.25
$\text{MgO}$	4.37	4.24	4.37	4.08	4.37	4.28	4.37	4.35	4.37	4.45
$\text{CaO}$	6.72	6.31	6.72	6.68	6.72	6.53	6.72	6.56	6.72	6.87
$\text{BaO}$	3.51	3.39	3.61	3.37	3.71	3.53	3.80	3.55	3.90	3.75
$\text{Fe}_2\text{O}_3$	3.43	3.58	3.40	3.47	3.38	3.35	3.35	3.43	3.32	3.28
$\text{La}_2\text{O}_3$	1.86	2.01	1.73	2.06	1.60	1.73	1.46	1.58	1.33	1.21
$\text{NiO}$	0.41	0.32	0.76	0.82	1.11	1.05	1.46	1.35	1.80	1.84
$\text{V}_2\text{O}_5$	1.50	1.54	1.50	1.43	1.50	1.38	1.50	1.53	1.50	1.55
$\text{SO}_3$	0.74	0.54	0.75	0.62	0.75	0.57	0.76	0.61	0.77	0.53
$\text{Sb}_2\text{O}_3$	0.50	0.56	0.50	0.59	0.50	0.53	0.50	0.56	0.50	0.48
Others **	0.88	0.62	0.76	0.63	0.65	0.51	0.55	0.58	0.45	0.52
Total	100.00	100.00	100.00	100.00	100.00	100.00	100.00	100.00	100.00	100.00

Note: \* The content of  $\text{B}_2\text{O}_3$  and  $\text{Li}_2\text{O}$  is not measured; \*\* Others include  $\text{Cr}_2\text{O}_3$ ,  $\text{K}_2\text{O}$ ,  $\text{ZrO}_2$ ,  $\text{P}_2\text{O}_5$ ,  $\text{MoO}_3$ ,  $\text{Cs}_2\text{O}$ ,  $\text{SrO}$ ,  $\text{CeO}_2$ , and  $\text{Y}_2\text{O}_3$ .

Sulfur retention is always a concern in vitrification because of the formation of detrimental yellow phases [1,3,21]. In this study, the sulfur content retained in the glasses fluctuated from 0.53 to 0.62 wt %, with a retention rate ranging from 68.8% to 82.7%, as plotted in Figure 2. As plotted in Figure 3, the glass density and the molar volume remained constant in the range of 2.72–2.74 g·cm<sup>-3</sup> and 23.8–24.0 cm<sup>3</sup>·mol<sup>-1</sup>, respectively, as the sludge content of the glass increased.

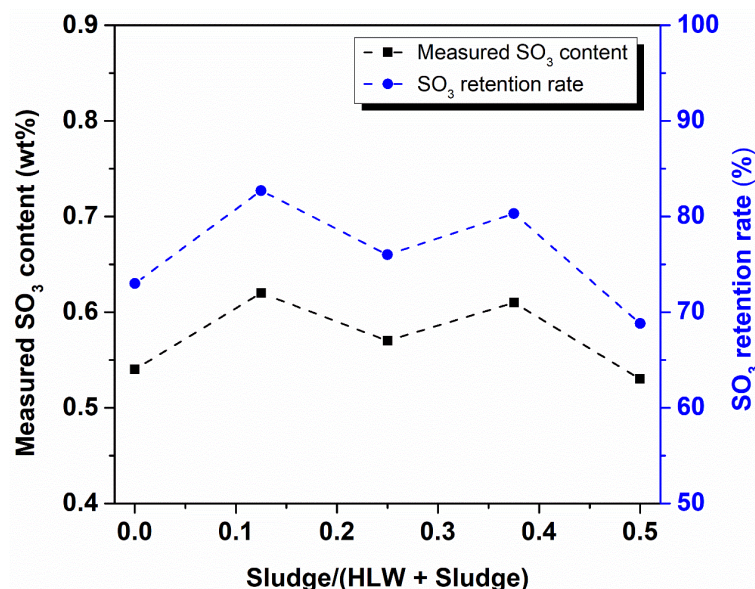


Figure 2. The measured SO<sub>3</sub> retention in glasses NJ0–NJ4.

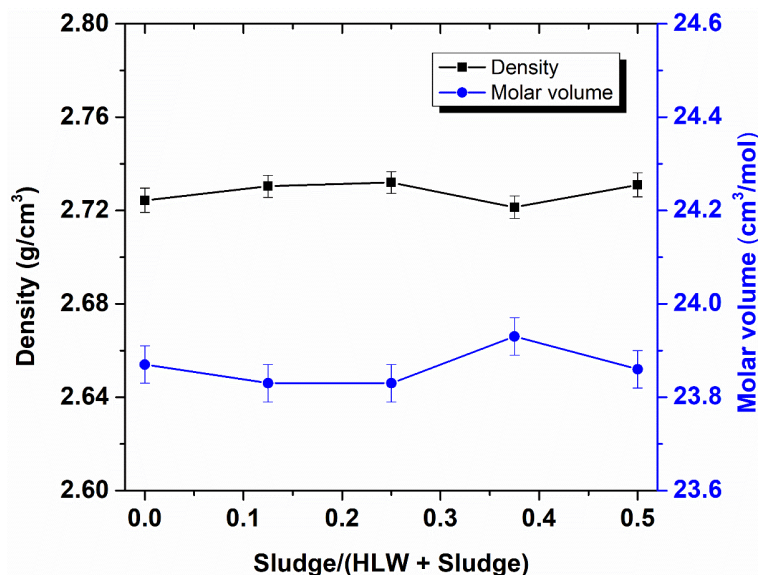


Figure 3. The density and molar volume of glasses NJ0–NJ4.

### 3.3. DSC Curves

Figure 4a illustrates the DSC curves of the prepared glasses. The glasses remained thermally stable up to the glass-transition temperature ( $T_g$ ), estimated from the onset of the first endothermic peak. Moreover, while the  $T_g$  of glasses NJ0–NJ2 was constant around 500 °C, it increased to 506 and 510 °C for glasses NJ3 and NJ4, respectively, as plotted in Figure 4b. The exothermic peak, indicating the glass crystallization temperature ( $T_c$ ), was at 800–900 °C. In addition, the intensity of the  $T_c$  peak gradually increased from glass NJ0

to glass NJ4, implying an increased tendency towards glass crystallization caused by the addition of the sludge.

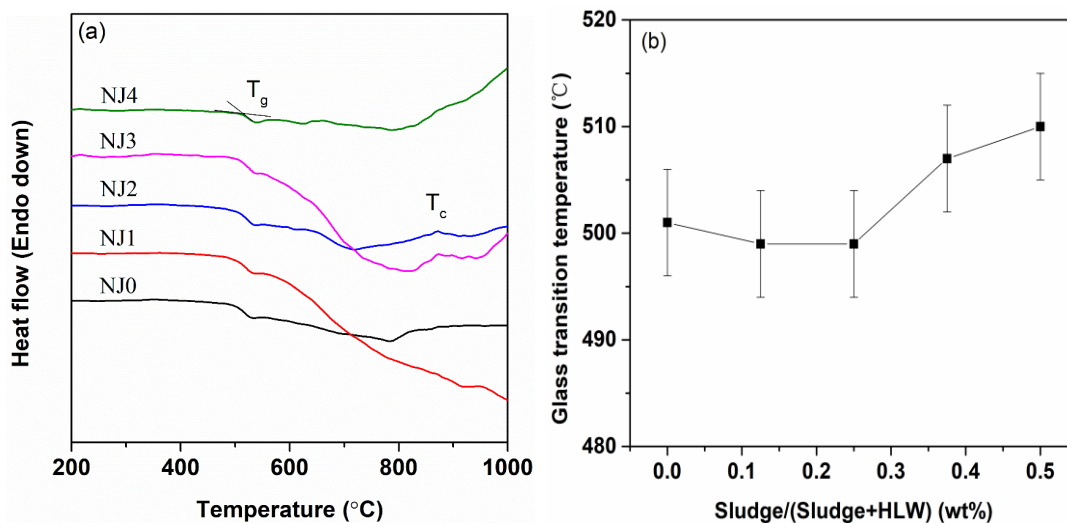


Figure 4. (a) The DSC curves of glasses NJ0–NJ4 and (b) the estimated  $T_g$  values.

### 3.4. Viscosity

Figure 5 presents the viscosity of the prepared glasses at 950–1150 °C. The viscosity of all five glasses steadily decreased exponentially with the increasing temperature, which agreed well with the widely used Arrhenius-type formula for the viscosity of Newtonian glass melts [1,22,23], as expressed below:

$$\ln(\eta) = A + B/T \tag{1}$$

where  $\eta$  represents the viscosity of the glass melts,  $A$  and  $B$  are the composition-related constants, and  $T$  indicates the temperature. The introduction of sludge to glass does not affect the Newtonian nature of glass melts at high temperatures.

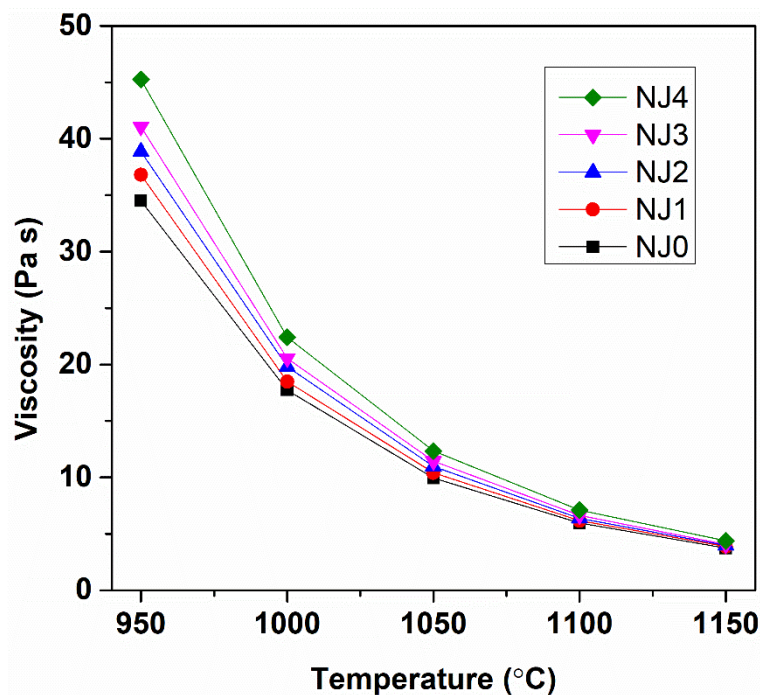


Figure 5. The high-temperature viscosity of glasses NJ0–NJ4.

Meanwhile, the viscosity of the glasses almost linearly increased with the increases in the sludge content: The viscosity increased from 3.74 Pa·s for glass NJ0 to 4.37 Pa·s for glass NJ4 at 1150 °C; at 950 °C, it increased from 34.52 Pa·s for glass NJ0 to 45.24 Pa·s for glass NJ4.

### 3.5. Glass-Crystallization Features

Figure 6 illustrates the XRD patterns of glasses NJ0–NJ4 after 24 h of heat treatment at different temperatures. Significant crystalline peaks can be observed for all the glasses thermally treated at 850–950 °C, and these peaks (at a  $2\theta$  of 19.8°, 27.6°, 29.9°, 30.3°, 30.9°, 35.0°, 35.5°, 35.8°, 39.2°, 40.7°, 42.0°, 42.5°, 43.0°, 44.3°, 44.9°, 52.4°, 56.7°, and 65.8°) agree well with the patterns of the diopside ( $\text{CaMgSi}_2\text{O}_6$ , PDF#72-1497), which was also the dominant crystalline phase in VPC glass [24,25]. No other crystalline phases were observed.

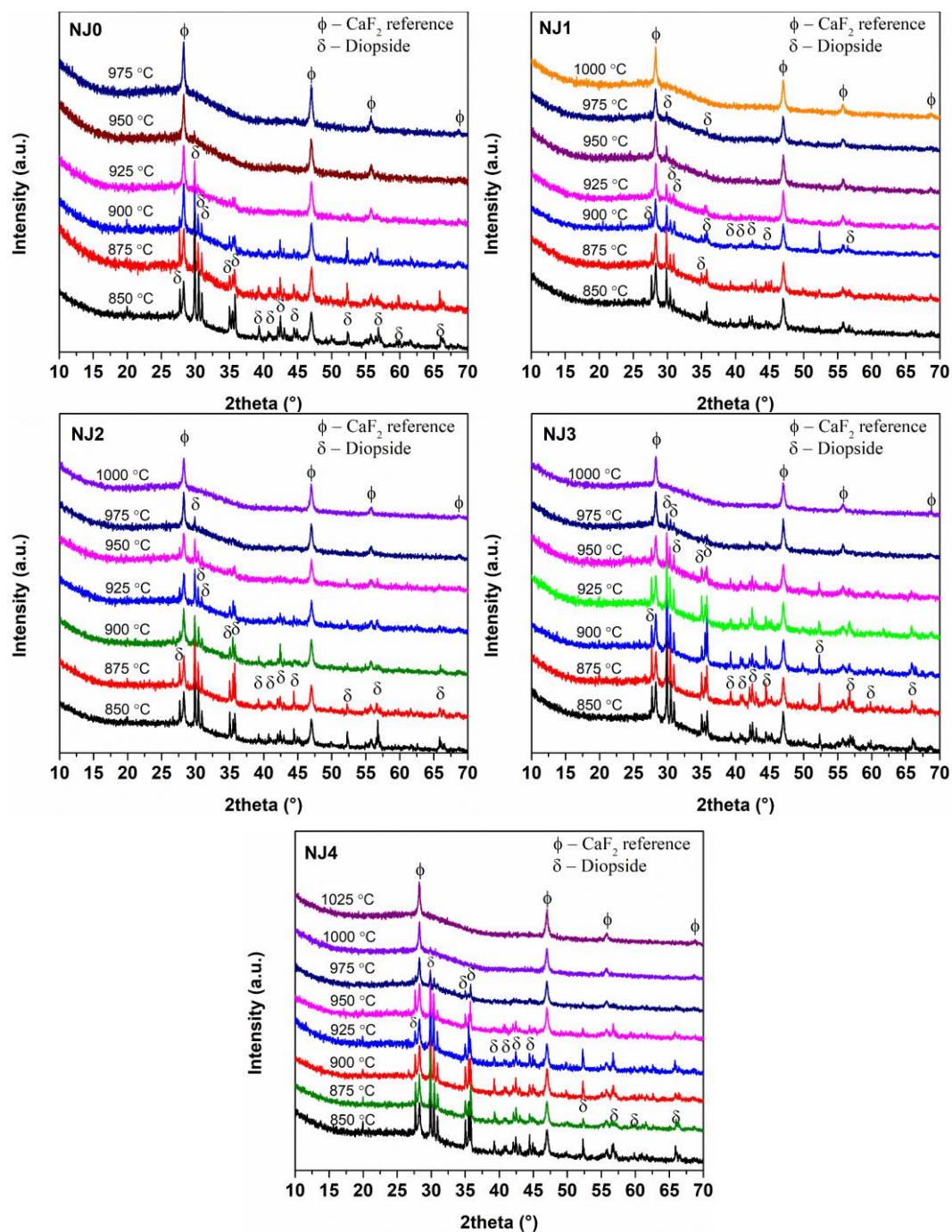
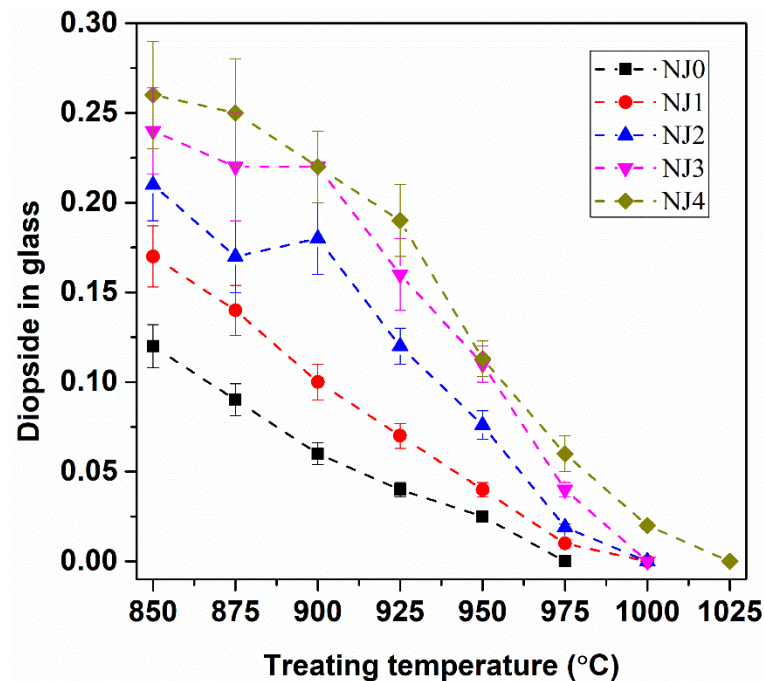


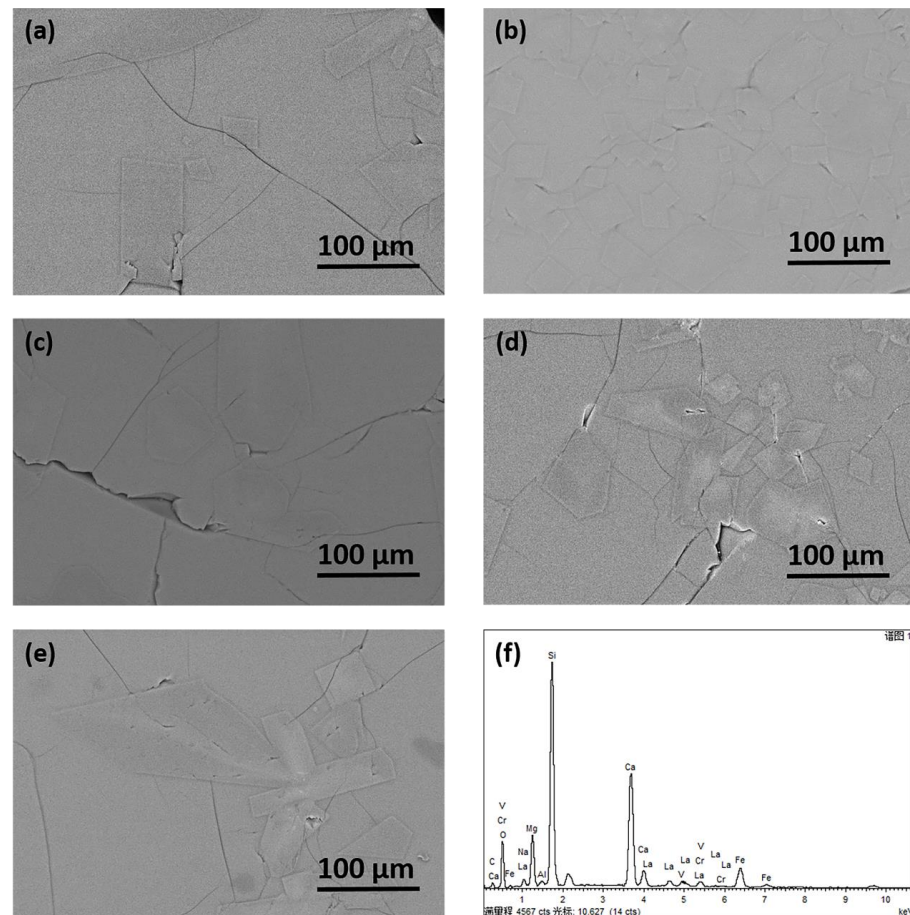
Figure 6. The XRD patterns of glasses NJ0–NJ4 when thermally treated for 24 h at different temperatures.

Figure 7 plots the results of the quantitative analysis of the crystallinity in the glasses. The content of diopside crystals in glass NJ0 linearly decreased from 12.3 wt % at 850 °C to 2.5 wt % at 950 °C, and, no crystals were formed during the heat treatment at 975 °C. The crystal content of glass NJ1 slightly increased compared to that of glass NJ0 at all the treatment temperatures, and the temperature at which the crystalline peaks disappeared changed to 1000 °C. The increasing tendency towards diopside crystallization continued with the increase in the simulated sludge contents of the glasses, and glass NJ4 had diopside contents of 26.0 wt % at 850 °C and 11.3 wt % at 950 °C, coupled with a glass liquidus temperature ( $T_L$ ) higher than 1000 °C.



**Figure 7.** The weight percentages of diopside in different crystallized glasses, as determined by the quantitative XRD analysis.

Figure 8 illustrates the backscattered electron (BSE) images of glasses NJ0–NJ4 after the heat treatment at 900 °C for 24 h. The formed crystals of all the glasses were tabular or plate-like and were randomly distributed within the glass matrices. These particles were generally greater than or equal to 100  $\mu\text{m}$  in length and tens of micrometers in width, with a tendency to agglomerate and form larger crystals. Figure 8f is a typical EDXS spectrum taken from the particles in glass NJ0 treated at 900 °C, demonstrating that these particles primarily comprised Si, Ca, Mg, Fe, Na, and O. Table 3 lists the normalized compositions of the particles formed in the different glasses. It should be pointed out that only the crystals in the glasses treated at 900 °C were analyzed, and our previous unpublished work showed that the compositions of diopside crystals formed in one glass treated at different temperatures are essentially the same. All the crystals had a stoichiometry close to that of the diopside  $\text{CaMgSi}_2\text{O}_6$ , with a significant substitution of Fe with Ca and Mg. In addition, the crystals contained small amounts of Al, Cr, Ni, and La.



**Figure 8.** The BSE images of the crystallized regions in glasses (a) NJ0, (b) NJ1, (c) NJ2, (d) NJ3, and (e) NJ4; (f) an EDXS spectrum taken from diopside crystals in the crystallized regions in glass NJ0. The Chinese word on the top-right means “Spectrum 1”. At the bottom the words mean “Full scale 4567 cts Cursor 10.627 (14 cts)”.

**Table 3.** The chemical compositions of the crystals in the glasses analyzed by EDXS.

Sample	Atomic Content (Normalized to O = 6; Fe Assumed to Be Present as Fe <sup>2+</sup> )								
	Si	Ca	Mg	Fe	Al	Cr	Ni	La	O
NJ0	2.05	0.77	0.80	0.20	0.02	0.02	0.01	0.03	6.00
NJ1	2.07	0.78	0.77	0.17	0.04	0.01	0.02	0.03	6.00
NJ2	2.07	0.76	0.78	0.19	0.03	0.02	0.02	0.02	6.00
NJ3	2.07	0.78	0.74	0.18	0.03	0.02	0.04	0.03	6.00
NJ4	2.06	0.75	0.77	0.18	0.04	0.01	0.04	0.04	6.00

### 3.6. PCT-B Test

Figure 9 plots the changes in the normalized leaching rates ( $NR_i$ ) of the Si, B, Na, and Cs from the different glasses after the 7-day PCT-B leaching test. As was typically found, B and Na were the major leaching elements, and the Si and Cs leached less. Further, increasing the sludge content of the glass steadily reduced the normalized leaching rates of these elements: The  $NR_{Na}$  was  $0.26 \text{ g}\cdot\text{m}^{-2}\cdot\text{d}^{-1}$  for glass NJ0 and rapidly dropped to  $0.12 \text{ g}\cdot\text{m}^{-2}\cdot\text{d}^{-1}$  for glass NJ4; however,  $NR_B$  was  $0.23 \text{ g}\cdot\text{m}^{-2}\cdot\text{d}^{-1}$  for glass NJ0 and gradually declined to  $0.15 \text{ g}\cdot\text{m}^{-2}\cdot\text{d}^{-1}$  for glass NJ4. The  $NR_{Si}$  also showed a decreasing tendency similar to that of the  $NR_B$ , but to a much lesser extent, declining from  $0.062$  to  $0.026 \text{ g}\cdot\text{m}^{-2}\cdot\text{d}^{-1}$ . The  $NR_{Cs}$  slightly decreased from  $0.12 \text{ g}\cdot\text{m}^{-2}\cdot\text{d}^{-1}$  for glass NJ0 to  $0.08 \text{ g}\cdot\text{m}^{-2}\cdot\text{d}^{-1}$  for glass NJ3, but it increased to  $0.09 \text{ g}\cdot\text{m}^{-2}\cdot\text{d}^{-1}$  for glass NJ4.

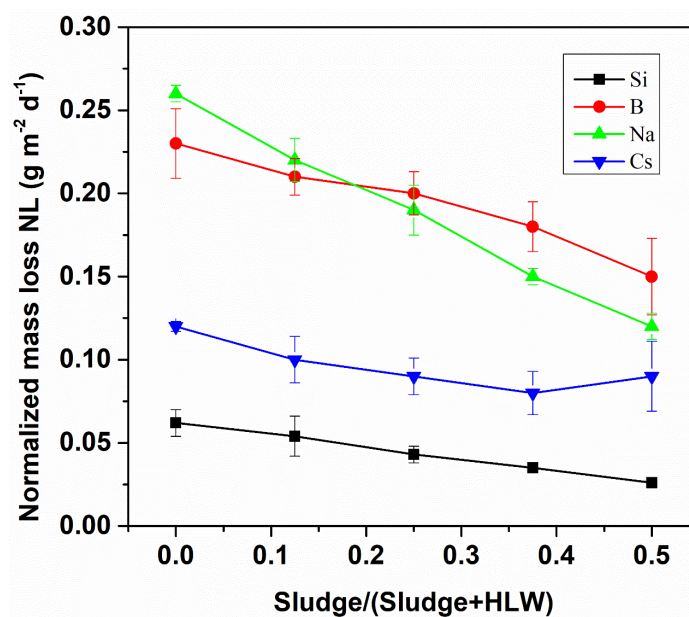


**Figure 9.** The normalized leaching-mass loss of Si, B, Na, and Cs of glasses NJ0–NJ4, according to the 7-day PCT–B leaching test.

#### 4. Discussion

##### 4.1. Influence of Sludge Content on Glass Products' Properties

All the prepared glasses were homogeneous and X-ray-amorphous, indicating that basic glass can tolerate the addition of at least 50 wt % of sludge to HLW at a given overall waste-oxide loading of 16 wt % (the level that is currently applied in VPC). Therefore, the capacity of glass to accommodate sludge content is not the factor that restricts the addition of sludge to HLW during vitrification.

Introducing sludge into glass leads to minor changes in glass density and molar volume. Compared with the HLW simulant, the sludge simulant contained more  $\text{Al}_2\text{O}_3$  and  $\text{BaO}$  and less  $\text{Na}_2\text{O}$  and  $\text{La}_2\text{O}_3$ . Both  $\text{BaO}$  and  $\text{La}_2\text{O}_3$  are prone to increasing glass densities due to the fact that they have greater mass than other components, and the influence of the addition of sludge to HLW on glass density is balanced by the increase in  $\text{BaO}$  content and the decrease in  $\text{La}_2\text{O}_3$  content.

It appears that the sulfur retention was not correlated with the increasing sludge content, although it is widely reported that sulfur solubility and retention behavior are determined by glass composition [26,27]. One possible explanation for this is that the fractions of  $\text{BaO}$ ,  $\text{CaO}$ ,  $\text{MgO}$ , and  $\text{V}_2\text{O}_5$  remained stable among the glasses, and they functioned as the principal oxides for determining the dissolution of the sulfur in the glass melts. The compositional variation herein, primarily  $\text{Al}_2\text{O}_3$ ,  $\text{Na}_2\text{O}$ , and  $\text{NiO}$ , was not influential. In addition, the sulfur-retention rates (0.5–0.6 wt %) in this study were close to the values reported in [5,28,29], in which sulfate-bearing wastes were vitrified in similar conditions. It is also worth noting that, although the sulfur retention rate was not particularly high, the “cold cap” and the bubbling stirrer applied in JHCMS can improve the further dissolution of sulfur into glass melts during vitrification.

The  $T_g$ s of all the glasses ranged between 500 and 510 °C, which suggests that the influence of sludge content on the thermal stability of glass is limited. However, the addition of sludge content does affect the crystallization behavior of glass. The crystals formed in the glass during the heat treatment were compositionally similar among the glasses; this was because the major compositional variations among the glasses were  $\text{Al}_2\text{O}_3$ ,  $\text{NiO}$ ,  $\text{Na}_2\text{O}$ , and  $\text{La}_2\text{O}_3$ , none of which play a vital role in diopside crystallization. The crystallization tendency linearly increased with the increasing addition of sludge content, which is likely to have been due to the increased  $\text{Al}_2\text{O}_3$  and  $\text{NiO}$  contents of the glass, which affected the glass-network stability. Borosilicate glasses containing high  $\text{Al}_2\text{O}_3$  contents

tend to crystallize when heated at specific temperatures [14,16,30], resulting in phase separations within the glass matrices, regardless of whether the phases contain Al. A small amount of NiO was found in the formed Fe-diopside crystals, according to the EDXS; thus, increasing NiO contents may enhance the overall crystallization of glasses. In addition, NiO is reported to degrade the thermal stability of glass networks and, therefore, support the crystallization of alkaline-earth borosilicate in CaO-SrO-Al<sub>2</sub>O<sub>3</sub>-B<sub>2</sub>O<sub>3</sub>-SiO<sub>2</sub> glasses [18,31], although it does not join the crystals.

The chemical durability of glass is improved by the addition of sludge content. This can be attributed to the increase in Al<sub>2</sub>O<sub>3</sub> content and the decrease in Na<sub>2</sub>O content in glass, which gives rise to enhanced glass-network connectivity [13]. Although BaO is reported to have a reduced impact on the chemical durability of glass [18], it may be overridden by the notable changes in Al<sub>2</sub>O<sub>3</sub> and Na<sub>2</sub>O contents. In addition, since the least durable glass (NJ0) had already been verified for chemical durability [20], all the glasses in this study were deemed to be sufficiently durable as high-level wasteforms.

In summary, basic glass can tolerate the addition of up to 50% sludge to HLW while maintaining similar or better glass properties.

#### 4.2. Influence of Sludge Content on Glass Melting

The increase in the viscosity of the glasses (~17% at 1150 °C and ~31% at 950 °C, from NJ0 to NJ4, respectively) with the addition of sludge can be attributed to the much higher content of Al<sub>2</sub>O<sub>3</sub> and lower content of Na<sub>2</sub>O in the simulated sludge, as reported elsewhere [23,32,33]. However, despite the apparent increase, the viscosity of all the glasses still fulfilled the suggested processing requirements (3–6 Pa·s at 1150 °C and 20–65 Pa·s at 950 °C). Nevertheless, this is likely to have caused the decreased fluidity of the glass melt in the melter and a decreased pouring rate for glass production, resulting in a longer duration requirement for glass residence and a long duration of glass pouring. Therefore, although the current processing parameters may still apply to the addition of sludge, the processing methods need to be modified along with their operation. If a variation in viscosity of less than 10% is needed, NJ1 and NJ2 glasses are more desirable.

The liquidus temperature  $T_L$  of the glass should be sufficiently low (e.g.,  $\leq 950$  °C) for no or few crystals to be present in glass melts at the temperatures set for pouring, so as to prevent the emergence of residual crystals in glass melts from the clogging of the discharge valve. In this study, the addition of sludge to the glass led to a notable increase in  $T_L$  (from 950–975 °C for glass NJ0 to 975–1000 °C for glasses NJ1–NJ3 and to 1000–1025 °C for glass NJ4). This increase was probably due to the increase in the Al<sub>2</sub>O<sub>3</sub> and NiO contents in the glass; NiO is reported to strongly increase  $T_L$  at ~80 °C per wt % in nuclear-waste glasses, and Al<sub>2</sub>O<sub>3</sub> increases  $T_L$  to a lesser extent [34,35]. Increases in  $T_L$  increases the risk of clogging glass melters, especially when glass melts are readily crystallized. Therefore, glasses NJ0–NJ2 are considered more acceptable, from the point of view of the liquidus temperature, for maintaining a low crystal content in glass melts at 950–975 °C.

As a result, the use of NJ0–NJ2 glasses, in which the ratio of sludge to HLW is from 0:8 to 2:6, is recommended to facilitate the glass melting process.

## 5. Conclusions

Borosilicate glasses containing different amounts of simulated HLW and sludge were successfully produced, with all the glasses being amorphous and homogeneous. From the above results and discussion, the following conclusions can be drawn:

- The substitution of sludge for HLW was conducive to minor changes in the glass density, molar volume, glass-transition temperature, and sulfur retention.
- The substitution of sludge for HLW gave rise to a notable increase in the viscosity and chemical durability of the glasses. Upon heat treatment, the crystallinity increased with the increasing sludge content in the glass, although the formed crystalline phases in the glasses remained the same.

- The glasses NJ0–NJ2 were proposed to vitrify the HLW blended with the sludge from the perspective of melter processing; that is, the sludge content in the overall waste should not exceed 25 wt %.

However, considering the varying compositions of the sludges in and among HLW tanks, the influence of individual elements in sludge on glass properties should also be determined. An acceptable range of compositional fluctuation is needed for application. In addition, optimization of basic glass formulations for mixed sludge and HLW vitrification was also studied in our recent work.

**Author Contributions:** Conceptualization, S.T.; methodology, J.C. and S.T.; data curation, X.L., J.C., S.T. and S.S.; writing—original draft preparation, S.T. and J.C.; writing—review and editing, S.T., S.S. and S.Z.; supervision, S.Z.; funding acquisition, L.X. All authors have read and agreed to the published version of the manuscript.

**Funding:** This research was funded by the China National Nuclear Corporation (CNNC) Youth Innovation Team Project, grant number FC192012000403, and SHIKUAN SUN appreciates the financial support from the National Natural Science Foundation of China under grant number 52172064.

**Institutional Review Board Statement:** Not applicable.

**Informed Consent Statement:** Not applicable.

**Data Availability Statement:** The data that support the findings of this study are available from the corresponding authors upon reasonable request.

**Acknowledgments:** We thank Tao Yu and Dongsheng Qie for the use of the laboratories for this study.

**Conflicts of Interest:** The authors declare no conflict of interest. The funders had no role in the design of the study; in the collection, analyses, or interpretation of data; in the writing of the manuscript; or in the decision to publish the results.

## References

- Ojovan, M.I. Immobilisation of Radioactive Wastes in Glass. In *An Introduction to Nuclear Waste Immobilisation*, 3rd ed.; Ojovan, M.I., Lee, W.E., Kalmykov, S.N., Eds.; Elsevier: Amsterdam, The Netherlands, 2019; pp. 319–368.
- Aloy, A.S. Calcination and vitrification processes for conditioning of radioactive wastes. In *Handbook of Advanced Radioactive Waste Conditioning Technologies*, 1st ed.; Ojovan, M.I., Ed.; Woodhead Publishing: Oxford, UK, 2011; pp. 136–158.
- Tan, S. Glass-based stabilization/solidification of radioactive waste. In *Low Carbon Stabilization and Solidification of Hazardous Wastes*; Tsang, D., Wang, L., Eds.; Elsevier: Amsterdam, The Netherlands, 2021; pp. 433–447.
- Wang, X.; Tuo, X.; Zhou, H.; Zhang, W.; Li, Z.; Chen, X.; Luo, H. Glass formulation development on high sodium and high sulfur bearing high level liquid waste for vitrification process. *J. Nucl. Radiochem.* **2013**, *35*, 180–192. (In Chinese)
- Wu, L.; Xiao, J.; Wang, X.; Teng, Y.; Li, Y.; Liao, Q. Crystalline phase, microstructure, and aqueous stability of zirconolite–barium borosilicate glass-ceramics for immobilization of simulated sulfate bearing high-level liquid waste. *J. Nucl. Mater.* **2018**, *498*, 241–248. [[CrossRef](#)]
- Liang, J.; Song, C.; Pan, C.; Ding, G.; Yang, W. The Preliminary Study of High-Level Radioactive Sludge I. Preparation and Property Study of Simulated High Level Radioactive Sludge. *J. Nucl. Radiochem.* **2000**, *22*, 37–44. (In Chinese)
- Fox, K.M.; Edwards, T.B.; Peeler, D.K. *High Level Waste (HLW) Sludge Batch (SB4)-Selecting Glasses for a Variability Study*; Savannah River National Laboratory: Aiken, SC, USA, 2006; p. 29.
- Sayenko, S.Y.; Shkuropatenko, V.A.; Pylypenko, O.V.; Karsim, S.O.; Zykova, A.V.; Kutnii, D.V.; Wagh, A.S. Radioactive waste immobilization of Hanford sludge in magnesium potassium phosphate ceramic forms. *Prog. Nucl. Energy* **2022**, *152*, 104315. [[CrossRef](#)]
- Donald, I.W. *Waste Immobilisation in Glass and Ceramic Based Hosts: Radioactive, Toxic and Hazardous Wastes*; Wiley-Blackwell: Chichester, UK, 2010; p. 527.
- Heath, P.G.; Stewart, M.W.A.; Moricca, S.; Hyatt, N.C. Hot-isostatically pressed wasteforms for Magnox sludge immobilisation. *J. Nucl. Mater.* **2018**, *499*, 233–241. [[CrossRef](#)]
- Tan, S.; Kirk, N.; Marshall, M.; McGann, O.; Hand, R.J. Vitrification of an intermediate level Magnox sludge waste. *J. Nucl. Mater.* **2019**, *515*, 392–400. [[CrossRef](#)]
- Amamoto, I.; Kobayashi, H.; Kitamura, N.; Takebe, H.; Mitamura, N.; Tsuzuki, T.; Fukayama, D.; Nagano, Y.; Jantzen, T.; Hack, K. Research on vitrification technology to immobilize radioactive sludge generated from Fukushima Daiichi power plant: Enhanced glass medium. *J. Nucl. Sci. Technol.* **2016**, *53*, 1467–1475. [[CrossRef](#)]
- Piovesan, V.; Bardez-Giboire, I.; Fournier, M.; Frugier, P.; Jollivet, P.; Montouillout, V.; Pellerin, N.; Gin, S. Chemical durability of peraluminous glasses for nuclear waste conditioning. *NPJ Mater. Degrad.* **2018**, *2*, 1–10. [[CrossRef](#)]

14. Mohd Fadzil, S.; Hrma, P.; Schweiger, M.J.; Riley, B.J. Component effects on crystallization of RE-containing aluminoborosilicate glass. *J. Nucl. Mater.* **2016**, *478*, 261–267. [[CrossRef](#)]
15. Mysen, B.; Richet, P. *Silicate Glasses and Melts*, 2nd ed.; Elsevier: Amsterdam, The Netherlands, 2018; p. 720.
16. Fox, K.M.; Peeler, D.K.; Edwards, T.B.; Best, D.R.; Reamer, I.A.; Workman, R.J.; Marra, J.C.; Riley, B.J.; Vienna, J.D.; Crum, J.V.; et al. *International Study of Aluminum Impacts on Crystallization in U.S. High Level Waste Glass*; Savannah River National Laboratory: Aiken, SC, USA, 2008; p. 172.
17. Cizman, A.; Idczak, K.; Krupinski, M.; Girsova, M.; Zarzycki, A.; Rysiakiewicz-Pasek, E.; Zielony, E.; Staniorowski, P.; Wrzesinska, P.; Perlikowski, I.; et al. Comprehensive studies of activity of Ni in inorganic sodium borosilicate glasses doped with nickel oxide. *Appl. Surf. Sci.* **2021**, *558*, 149891. [[CrossRef](#)]
18. Ren, M.; Yang, P.; Xu, J.; Zhang, Q.; Chen, K.; Tang, D.; Zhuang, H.; Sa, B.; Zhang, T. Effect of nickel doping on structure and suppressing boron volatility of borosilicate glass sealants in solid oxide fuel cells. *J. Eur. Ceram. Soc.* **2019**, *39*, 2179–2185. [[CrossRef](#)]
19. Mishra, R.K.; Sudarsan, K.V.; Sengupta, P.; Vatsa, R.K.; Tyagi, A.K.; Kaushik, C.P.; Das, D.; Raj, K. Role of Sulfate in Structural Modifications of Sodium Barium Borosilicate Glasses Developed for Nuclear Waste Immobilization. *J. Am. Ceram. Soc.* **2008**, *91*, 3903–3907. [[CrossRef](#)]
20. Liu, L.; Qie, D.; Zhou, H.; Li, B.; Li, Y.; Xu, J.; Zhang, H. Verification experiment research of glass formulation for high sodium and high sulfur bearing HLLW. *J. Nucl. Radiochem.* **2014**, *36*, 163–168. (In Chinese)
21. Goel, A.; McCloy, J.S.; Pokorny, R.; Kruger, A.A. Challenges with vitrification of Hanford High-Level Waste (HLW) to borosilicate glass—An overview. *J. Non-Cryst. Solids X* **2019**, *4*, 100033. [[CrossRef](#)]
22. Ojovan, M.I. Viscosity and Glass Transition in Amorphous Oxides. *Adv. Condens. Matter Phys.* **2008**, *2008*, 1–23. [[CrossRef](#)]
23. Hrma, P.; Kruger, A.A. High-temperature viscosity of many-component glass melts. *J. Non-Cryst. Solids* **2016**, *437*, 17–25. [[CrossRef](#)]
24. Meng, B.; Zhu, Y.; Yang, D.; Cui, Z.; Jiao, Y.; Liu, H.; Dai, C. Effect of alkaline earth metal oxide content on crystallization behavior of simulated high level liquid waste glass. *Bull. Chin. Ceram. Soc.* **2022**, *41*, 4081–4088.
25. Yang, Y.-G.; Zhang, Z.-T.; Hua, X.-H.; Wang, L. Crystallization of the simulated HLW glass. *J. Nucl. Radiochem.* **2014**, *36*, 317–320. (In Chinese)
26. Manara, D.; Grandjean, A.; Pinet, O.; Dussossoy, J.L.; Neuville, D.R. Sulfur behavior in silicate glasses and melts: Implications for sulfate incorporation in nuclear waste glasses as a function of alkali cation and V<sub>2</sub>O<sub>5</sub> content. *J. Non-Cryst. Solids* **2007**, *353*, 12–23. [[CrossRef](#)]
27. Lenoir, M.; Grandjean, A.; Poissonnet, S.; Neuville, D.R. Quantitation of sulfate solubility in borosilicate glasses using Raman spectroscopy. *J. Non-Cryst. Solids* **2009**, *355*, 1468–1473. [[CrossRef](#)]
28. Billings, A.L.; Fox, K.M. Retention of Sulfate in Savannah River Site High-Level Radioactive Waste Glass. *Int. J. Appl. Glass Sci.* **2010**, *1*, 388–400. [[CrossRef](#)]
29. Lorier, T.H.; Reamer, I.A.; Workman, R.J. *Initial Sulfate Solubility Study for Sludge Batch 4 (Sb4)*; Savannah River National Laboratory: Aiken, SC, USA, 2005; p. 22.
30. McClane, D.L.; Amoroso, J.W.; Fox, K.M.; Kruger, A.A. Nepheline crystallization behavior in simulated high-level waste glasses. *J. Non-Cryst. Solids* **2019**, *505*, 215–224. [[CrossRef](#)]
31. Mahapatra, M.K.; Lu, K. Effects of nickel on network structure and thermal properties of a new solid oxide cell seal glass. *J. Power Sources* **2008**, *185*, 993–1000. [[CrossRef](#)]
32. Hrma, P.; Han, S.-S. Effect of glass composition on activation energy of viscosity in glass-melting-temperature range. *J. Non-Cryst. Solids* **2012**, *358*, 1818–1829. [[CrossRef](#)]
33. Kroll, J.O.; Nelson, Z.J.; Skidmore, C.H.; Dixon, D.R.; Vienna, J.D. Formulation of high-Al<sub>2</sub>O<sub>3</sub> waste glasses from projected Hanford waste compositions. *J. Non-Cryst. Solids* **2019**, *517*, 17–25. [[CrossRef](#)]
34. Hrma, P.; Vienna, J.; Crum, J.; Piepel, G.; Mika, M. Liquidus Temperature of High-Level Waste Borosilicate Glasses With Spinel Primary Phase. *MRS Online Proc. Libr.* **1999**, *608*, 671. [[CrossRef](#)]
35. Jantzen, C.M.; Brown, K.G. Predicting the Spinel?Nepheline Liquidus for Application to Nuclear Waste Glass Processing. Part I: Primary Phase Analysis, Liquidus Measurement, and Quasicrystalline Approach. *J. Am. Ceram. Soc.* **2007**, *90*, 1866–1879. [[CrossRef](#)]

**Disclaimer/Publisher's Note:** The statements, opinions and data contained in all publications are solely those of the individual author(s) and contributor(s) and not of MDPI and/or the editor(s). MDPI and/or the editor(s) disclaim responsibility for any injury to people or property resulting from any ideas, methods, instructions or products referred to in the content.